Runoff response to spatial variability in precipitation: an analysis of observed data

Michael B. Smith[a],*, Victor I. Koren[a], Ziya Zhang[a], Seann M. Reed[a],
Jeng-J. Pan[b], Fekadu Moreda[a]

[a]*Hydrology Laboratory, Office of Hydrologic Development, WOHD-12 NOAA/National Weather Service,
1325 East–West Highway, Silver Spring, MD 20910, USA*
[b]*Centers for Medicare and Medicaid Services, 7500 Security Blvd, Baltimore, MD 21244, USA*

Abstract

We examine the hypothesis that basins characterized by (1) marked spatial variability in precipitation, and (2) less of a filtering effect of the input rainfall signal will show improved outlet simulations from distributed versus lumped models. Basin outflow response to observed spatial variability of rainfall is examined for several basins in the Distributed Model Intercomparison Project. The study basins are located in the Southern Great Plains and range in size from 795 to 1645 km^2. We test our hypothesis by studying indices of rainfall spatial variability and basin filtering. Spatial variability of rainfall is measured using two indices for specific events: a general variability index and a locational index. The variability of basin response to rainfall event is measured in terms of a dampening ratio reflecting the amount of filtering performed on the input rainfall signal to produce the observed basin outflow signal. Analysis of the observed rainfall and streamflow data indicates that all basins perform a range of dampening of the input rainfall signal. All basins except one had a very limited range of rainfall location index. Concurrent time series of observed radar rainfall estimates and observed streamflow are analyzed to avoid model-specific conclusions. The results indicate that one basin contains complexities that suggest the use of distributed modeling approach. Furthermore, the analyses of observed data support the calibrated results from a distributed model.
© 2004 Elsevier B.V. All rights reserved.

Keywords: Rainfall; Spatial variability; Dampening; Hydrologic response; Streamflow variability; NEXRAD; Radar; Precipitation; Wavelet transformation; Distributed model

1. Introduction and problem description

Several reasons exist for the application of distributed hydrologic models to a basin. To begin, such approaches offer the opportunity to model processes such as water balance, non-point sediment and pollution transport, and discharge at points upstream of the basin outlet. Moreover, distributed models can take advantage of the expanding number of new and emerging spatial data sets made possible by geographic information system capabilities and sensors aboard aircraft and satellites. A major reason for the use of distributed approaches is the hypothesis

that by accounting for the spatial variability of rainfall and physical features within the basin, better simulations can be achieved at the basin outlet. Many studies directly or indirectly investigated this hypothesis using models and/or synthetic rainfall data (e.g. Krajewski et al., 1991; Milly and Eagleson, 1988; Beven and Hornberger, 1982; Shanholtz et al., 1981; Wilson et al., 1979). However, recent studies (Carpenter et al., 2001; Smith et al., 1999; Bell and Moore, 1998; Seyfried and Wilcox, 1995; Obled et al., 1994; Pessoa et al., 1993; Naden, 1992) and more recently the results from Distributed Model Inter-comparison Project (DMIP) (see Reed et al., 2004, this issue) suggest that distributed modeling approaches may not always provide improved outlet simulations compared to lumped conceptual models.

At least part of the dilemma surrounding the lack of gains from distributed models may be attributed to errors in data, model structure, and model parameters (Koren et al., 2003; Carpenter et al., 2001; Carpenter and Georgakakos, 2004, this issue). The non-linearities and/or many computational elements in distributed models may magnify rather than smooth errors in high-resolution radar rainfall data, making it difficult for distributed models to outperform a well-calibrated lumped model in cases of uniform precipitation.

More subtly, another aspect of this conundrum is that many of the past studies on the importance of the spatial variability to basin response relied on simulations and have perhaps implicitly and unduly stressed *model* sensitivity and not observed *basin* sensitivity (Morin et al., 2001; Winchell et al., 1998; Obled et al., 1994). For example, both Obled et al. (1994) and Bell and Moore (2000) noted spurious simulated hydrograph peaks where none were present in the observed streamflow. As pointed out by Winchell et al. (1998) in their review of past studies, the conclusion has been that runoff-generation is highly sensitive to the spatial and temporal variability of rainfall. In their review, however, they identified a strong bias in the use of the infiltration-excess runoff-generation mechanism in these sensitivity studies. Moreover, the few studies that did use the saturation-excess type of runoff mechanism did not support the general conclusion from the other modeling studies regarding the importance of rainfall spatial variability.

The work by Winchell et al. (1998) seems to confirm the model results and postulates of Obled et al. (1994).

In their attempt to capture the spatial variability of precipitation, Obled et al. (1994) observed that their *model* sometimes responded to a rainfall event which the *basin* ignored or dampened. Obled et al. (1994) highlighted the problem of how well a model structure and parameters fit the real system when making conclusions from *simulation* studies. Furthermore, they noted that in medium sized catchments (from 100 to a few 1000 km^2), most proofs for the significance of the rainfall pattern were based on synthetic studies. They went on to suggest that if the dominant runoff-generation process is of the Dunne type rather than the Hortonian, then most of the rainfall infiltrates and will be smoothed out as the water is stored and delayed in the soil layers. As an example, Milly and Eagleson (1988) found that when the infiltration-excess mechanism is dominant, then the rainfall/runoff process is highly sensitive to storm scale.

Arnaud et al. (2002) tried to avoid conclusions based on specific runoff-generation mechanisms by using a distributed model with three rainfall-runoff schemes. In a study with observed rainfall applied to fictitious basins, they concluded that runoff volumes and peak flows can vary considerably between spatially uniform and spatially distributed rainfall patterns.

Yet, another aspect of this puzzle (and one we investigate here) is that perhaps the spatial variability and organization of rainfall, while present, may not be great enough to produce variability in the observed basin response. As Obled et al. (1994) stated:

"In fact, it seems that the spatial variability of rainfall, although important, is not sufficiently organized in time and space to overcome the effect of smoothing and dampening when running off through this rural medium sized catchment".

Several other studies have examined the spatial variability of rainfall in the context of overcoming the dampening action of a basin. Bell and Moore (2000) explored this issue by comparing the sensitivity of basin runoff to two types of rainfall events. The authors found much greater runoff variability for convective as opposed to stratiform rainfall, noting the significant dampening and reduced runoff variability during stratiform events. Woods and Sivapalan (1999) noticed the failure of substantial

spatial variations of rainfall in (x, y) coordinates to impose any significant influence on the variability in the timing of catchment response. They attributed this to the limited variability of rainfall with flow distance from the basin outlet. In her examination of the Thames River basin, Naden (1992) found that the hillslope response was dominant over the channel routing response and masked any effect of the marked spatial variability of rainfall. Apparently, the large proportion of chalk and limestone in the catchment caused the hillslope dominance. Runoff moving through the catchment had a much longer residence time in the hillslope component versus the channel system. Catchment response functions for seven events were very similar despite observed spatial variability in precipitation. She concluded that a semi-distributed modeling approach did not provide a significant improvement over a lumped model applied to this 7000 km^2 catchment.

In light of these recent studies, it does not appear sufficient to simply determine where great spatial variability of rainfall and physical basin character-istics exists, but to identify basins in which the variability of rainfall forcing *overcomes* any filtering by the physical basin to result in significant variability of the basin response. Perhaps when this latter condition is met, distributed models can be shown to reliably improve upon lumped model results.

We provide an overview of the paper as follows. In Section 2, we develop our hypothesis and define the limits of our study. Following this, we briefly discuss the data in Section 3. In Section 4, we develop three indices based on observed data. A brief overview of wavelet analysis is also provided. In Section 5, we evaluate various combinations of the indices of spatial variability and basin filtering, followed by the analysis of the National Weather Service (NWS) distributed and lumped model simulations. We state our study conclusions in Section 6, and make recommendations for further study in Section 7.

2. Purpose and scope

Given the effort to implement a physically based distributed model, and the emerging reality that distributed model may not improve upon lumped models in all cases (Seyfried and Wilcox, 1995), it is important to determine in which basins the spatial variability of rainfall results in corresponding varia-bility in outflow response (Bell and Moore, 2000). In this paper, we analyze observed rainfall and stream-flow to describe the spatial variability of rainfall and corresponding basin outflow response in order to make inferences about model applicability, specifi-cally, the need for distributed versus lumped models. We exclude effects of model error as well as data and parameter uncertainty.

Based on the conclusions of Obled et al. (1994) and other discussions in Section 1, we formulate the following hypothesis:

> Basins characterized by (1) spatial variability of precipitation and (2) less filtering of the rainfall signal will be more amenable to distributed modeling.

Here, we define 'amenable' to mean that the distributed model provides improvement over a lumped model for basin outlet simulations. To test this hypothesis, we propose several indices for quantifying observed basin outflow sensitivity and spatially variable precipitation. Rather than using a model to evaluate a basin's response to spatially variable precipitation, we follow the intent of Jakeman and Hornberger (1993) and attempt to determine:

> "what reliable information may reside in concur-rent observed precipitation-streamflow measure-ments for assessing the dynamic characteristic of catchment response"

We develop diagnostic (rather than prognostic) indicators that in combination, can be used to formulate inferences on the nature of a basin's response. As much as possible, these indices are derived from observed data in order to avoid model-specific conclusions.

Using these diagnostic indices, we then attempt to answer the question: 'Does the combination of the computed indices and the distributed and lumped simulations from DMIP support our hypothesis?'

While we stress the analysis of observed precipi-tation/streamflow data, we recognize that to fully evaluate our hypothesis, we cannot avoid the use of

distributed and lumped model simulations. Therefore, we recognize that our conclusions are at least in part model-specific. Nonetheless, we argue that our emphasis on using observed data to first quantify basin outflow sensitivity has merit.

The analyses herein are limited to the mid-to-large size basins within the DMIP study area. Smith et al. (2004, this issue) provide a discussion of the study basins. In addition, we rely on others (Carpenter and Georgakakos, 2004, this issue; Carpenter et al., 2001) to comment on the effects of data and model parameter errors when evaluating lumped and distributed modeling results.

3. Data

We limit our study to the data pertinent to the DMIP project. Provisional hourly observed discharge data from the US Geological Survey (USGS) and placed on the DMIP web site were used. We use the gridded 4 km resolution NEXRAD data also provided on the DMIP website. Numerous studies have investigated the quality of these rainfall data for hydrologic modeling. The interested reader is referred to Smith et al. (2004, this issue), Reed et al. (2004, this issue), Guo et al. (2004, this issue), Young et al. (2000), and Wang et al. (2000) for more information. We use the hourly, gridded NEXRAD rainfall estimates to compute two indices of rainfall spatial variability. To compute the basin filtering index, the NEXRAD 4 km radar rainfall estimates were processed to create hourly time series of mean areal rainfall over each of the study basins. These mean areal time series were the same used to generate the lumped model simulations for DMIP.

As discussed earlier, we rely in part on model simulations to evaluate our hypothesis. We use the calibrated NWS distributed model results submitted to DMIP (see Reed et al., 2004, this issue), as well as the calibrated simulations from the NWS lumped model used as a standard in DMIP (Smith et al., 2004, this issue).

In this study, we analyze three DMIP basins, named after their respective USGS gage locations: Baron Fork at Eldon, Oklahoma; the Illinois River at Watts, Oklahoma, and the Blue River at Blue, Oklahoma. Hereafter, we refer to these basins as Eldon, Watts, and Blue, respectively.

4. Methodology

In this section, we explore the comments by Obled et al. (1994) regarding the conditions that rainfall must have both spatial variability and significant organization in order to overcome basin filtering to produce variability in outflow response. The analyses herein benefits from the use of high-resolution gridded radar rainfall estimates and corresponding hourly streamflow observations available through the DMIP project. We develop a specific index for general rainfall organization, rainfall variability, and variability in the basin outflow response.

4.1. Measures of rainfall variability

4.1.1. Index of rainfall location
This index quantifies the location of storms independent of intrastorm spatial variability of precipitation. Here, we attempt to describe the variability of rainfall versus channel flow distance as emphasized by Woods and Sivapalan (1999) and to investigate the spatial organization of rainfall (as opposed to rainfall spatial variability) as called for by Bell and Moore (2000)

To derive this index, we modify the rainfall centroid ratio proposed by Wei and Larson (1971) so that distance is measured along flow paths to the outlet and not in Euclidean coordinates. For this study, flow paths were estimated using a grid network at the resolution of the 4 km NEXRAD cells. The 4 km network was derived by generalizing information in a 30 m DEM (Reed, 2003). Based on gridded rainfall data shown in Fig. 1, a center of rainfall mass for each time step can be calculated in Eq. (1).

$$C_{\mathrm{pcp}} = \frac{\sum_{i=1}^{N} P_i A_i L_i}{\sum_{i=1}^{N} P_i A_i} \tag{1}$$

where P_i is rainfall amount at grid i, L_i is the distance of grid i to the basin outlet, A_i is the area of grid i, and N is the total number of grid cells within the basin. Distance L_i is measured along overland and catchment flow paths defined by DEM analysis. Grid area A_i is retained in Eq. (1) to remind the reader that the area of each NEXRAD grid cell varies slightly with latitude. The unique area of each grid cell is used in the computation of this index and in the distributed model
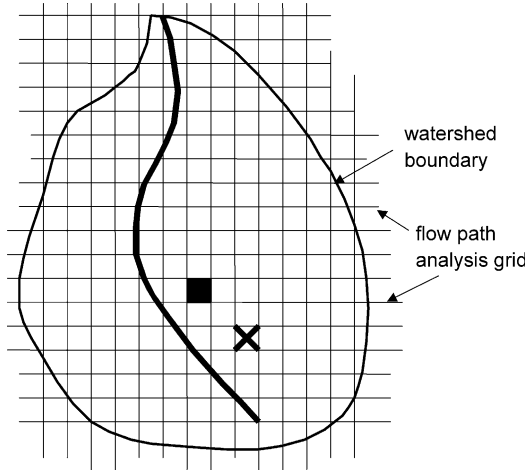
Fig. 1. Illustration of the rainfall location index. Shaded cell is the basin flow path centroid. The X cell has a location index greater than 1.0, as it is farther from the basin outlet than the centroid.

developed by the NWS Hydrology Laboratory and used in DMIP.

A basin's center of mass C_{bsn} can be calculated by the same way as above, except that $P_i = 1$. The rainfall centroid ratio for each time step can then be expressed as a dimensionless index using Eq. (2):

$$I_{pcp} = \frac{C_{pcp}}{C_{bsn}} \tag{2}$$

For a specific time, if $I_{pcp} < 1$, then the heavier rainfall for this time step is generally located at the region closer to the outlet. Values greater than 1.0 indicate that the center of rainfall is away from the outlet. I_{pcp} values near 1.0 imply that the rainfall is concentrated near the basin centroid.

For a specific event, the flow response is from many hours of rainfall before and possibly during the runoff. A location index (weighted rainfall centroid ratio) for a rainfall event of length T hours can be determined by weighting the rainfall amount during the period as:

$$I_L = \frac{\sum_{t=1}^{T} I_{pcp,t} P_t}{\sum_{t=1}^{T} P_t} \tag{3}$$

where $I_{pcp,t}$ is the rainfall location index for one time step t, and P_t is the spatially averaged rainfall amount for the same time step.

4.1.2. Index of general rainfall variability

To quantify intrastorm rainfall variability, we propose a general rainfall variability measure:

$$\sigma_t = \sqrt{\frac{\sum_{i=1}^{N} P_i^2}{N} - \frac{\left(\sum_{i=1}^{N} P_i\right)^2}{N^2}} \tag{4}$$

where all notations are the same as in the discussion of the locational index C. The quantity σ_t is basically the standard deviation of the hourly gridded NEXRAD rainfall estimation covering a basin. Analogous to the index I_L, the index of rainfall variability over the entire flood event can be estimated as a weighted value I_σ:

$$I_\sigma = \frac{\sum \sigma_t P_t}{\sum P_t} \tag{5}$$

4.1.3. Measures of basin dampening

Corresponding to the measures of rainfall spatial variability, we seek an index of outflow hydrograph variability. Here, we define outlet hydrograph variability in terms of the amount of filtering or dampening performed on the input rainfall signal as shown in Fig. 2. This cross-analysis characterizes the transformation of an input signal into an output signal (Padilla and Pulido-Bosch, 1995). The shape of the output hydrograph is the result of the combined effects of all watershed processes such as interception, depression storage, infiltration, overland flow, storage and movement of water in the soil, and channel flow attenuation given the antecedent moisture conditions. Moreover, the effects of spatial variability of precipitation are implicitly present in the transformation in Fig. 2.

Others have analyzed hydrologic systems in terms of the filtering of the rainfall signal. Kisiel (1969) described a basin as a system that filters the high-frequency components of the input by smoothing out the amplitude of the rainfall. Padilla and Pulido-Bosch (1995), Angelini (1997), Larocque et al. (1998), and Labat et al. (2000a,b) used signal analysis techniques to describe the filtering aspects of karst aquifers. Shah et al. (1996) acknowledged that basins generally act to smooth or integrate rainfall in both time and space, and stated that the complex relationships between the degree of spatial variability of rainfall, basin physical
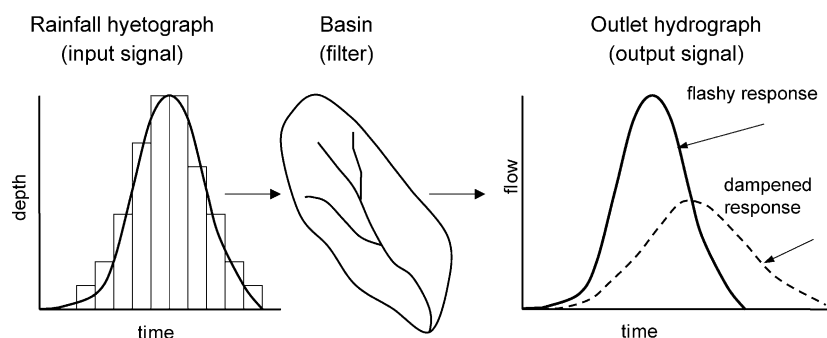
Fig. 2. Transformation of the input signal (rainfall hyetograph) to output signal (discharge hydrograph). Two output signal responses are illustrated.

properties, antecedent moisture, and other factors are poorly understood. They went on to suggest that physically based distributed modeling systems could be used to explore these relationships. With their suggestions, however, they cautioned that these models can only be used given that accurate estimates of rainfall spatial distribution are available and the distributed model realistically represents the processes occurring naturally in the basin. Morin et al. (2002) studied the smoothing effects of the basin on the rainfall signal in order to define a new characteristic descriptor termed the response time scale (RTS) of a basin. The RTS is determined by averaging the rainfall signal over increasingly longer intervals, so that the time interval range providing a smoothed rainfall signal with the best correlation to the runoff response is the RTS. The RTS analysis results in a rather coarse, but robust, range of values rather than a singular value for an individual event. Morin et al. (2003) applied the RTS concept to individual hydrological processes.

Here, like Morin et al. (2002), we avoid the question of the model 'correctness' raised by several authors (e.g. Berger and Entekhabi, 2001; Morin et al., 2001; Shah et al., 1996; Larson et al., 1994; Obled et al., 1994) and instead concentrate on the analysis of observed data to derive a descriptive index of basin dampening. For the input signal, we chose the time series of basin mean areal hourly rainfall computed from the NEXRAD radar rainfall estimates, while hourly observations of basin outlet discharge from the USGS are used as the output signal.

Clearly, the use of time series of basin mean areal rainfall may be questioned in a study on the spatial variability of precipitation. However, we caution the reader to note that the mean areal time series is used only as a measure of the volume per time input of the rainfall into the system. We rely on the indices I_L and I_σ to explicitly describe the spatial variability of precipitation. Most importantly, as shown later, we examine relationships amongst the three indices as the basis for inferences rather than relying on a single index to derive conclusions. Moreover, our analysis is not unlike that of Morin et al. (2002), who used mean areal rainfall values from radar time series in the computation of the RTS. They showed that mean areal values were probably appropriate for the small size (10–50 km^2) basins used in their study, even though some degree of smoothing may have already taken place. In our case, the use of mean areal averages of precipitation may be more critical given the spatial averaging of radar rainfall over larger basins sizes as seen in Fig. 2 of Finnerty et al. (1997). However, as this is an initial study, the use of basin mean areal precipitation values is probably valid for evaluating the use of the derived indices for making inferences about basin behavior. We discuss using other representations of the rainfall signal in Section 7.

Concepts from the relatively recent development of wavelet analysis are adapted to derive a single quantitative index that measures the amount of dampening of the input rainfall signal as it is transformed into runoff at the basin outlet as shown in Fig. 2. While other measures have been used to assess runoff variability (Bell and Moore, 2000; Woods and Sivapalan, 1999; Ogden and Julien, 1993), we explore wavelet transforms to derive a composite measure of rainfall signal dampening for

an event. We seek a diagnostic measure which represents the effects of all the processes beginning in time with the onset of rainfall and ending with the passing of the hydrograph recession limb at the basin outlet. This is in contrast to the RTS statistic (Morin et al., 2002), which uses the time duration of only the rising limbs of the rainfall hyetograph or discharge hydrograph.

Wavelet transformation represents the next step beyond a windowed Fourier transform in the analysis of times series. Like Fourier transforms, wavelet analysis reveals structures that may not be evident in the data when plotted in time–amplitude space. As Fourier analysis consists of decomposing signals into constituent sinusoids, wavelet analysis is the breaking up of a signal into scaled and translated versions of the original (or mother) wavelet. A wavelet transformation is a series of bandpass filters of the time series. Wavelets allow for long time periods where more precise low-frequency information is needed, and short time windows when detailed information is required. Wavelet analysis has gained in utility as seen by the rainfall decomposition work of Kumar and Foufoula-Georgiou (1990, 1993) and Smith et al. (1998) who used discrete wavelet transforms to characterize a number of rivers in five climatic regimes and to identify features not readily detected by Fourier analysis. Saco and Kumar (2000) extended this work by providing a comprehensive understanding of streamflow variability throughout the coterminous United States. Cahill (2002) used a wavelet-based test to identify changes in streamflow variance. While a detailed description of wavelet analysis is well beyond the scope of this paper, a brief overview here is necessary to explain our use of wavelet scale to derive a basin-event descriptor. Interested readers are referred to Torrence and Compo (1998) for more background. Gaucherel (2002) provides an excellent figure describing the correspondence of wavelets of various scales to different segments of a hydrograph.

The continuous wavelet transform of a discrete function or signal is defined as the convolution of the signal $s(t)$ with scaled and translated version of the function g, called the mother wavelet, as shown in Eq. (6) (Meyers et al., 1993; Smith et al., 1998):

$$Ws(b, a) = \frac{1}{\sqrt{a}} \int_{-\infty}^{+\infty} g\left(\frac{t - b}{a}\right) s(t) dt \qquad (6)$$

where Ws is the transformation of the signal or function $s(t)$, a is a scaling or dilation parameter, b is a location or translation parameter, t is time or distance, and g is the mother wavelet. Scaled and translated versions of the mother wavelet are called daughter wavelets or simply wavelets. Eq. (6) is known as a *continuous* wavelet transform since parameters a and b may be varied continuously. In *discrete* wavelet analysis, a and b are varied as powers of 2 (the so-called dyadic scales). Parameter b corresponds to time or position if a signal is a function of time or space, respectively, while a is related to scale or temporal period. The result of the wavelet transformation in Eq. (6) is a number of coefficients $Ws(b, a)$ which represent a local measure of the relative amplitude of activity at (b, a) and combines information on both the signal and wavelet. Convolution of a signal $s(t)$ of length N with a set of M scaled wavelets results in an array of M magnitude vectors, also of length N. Plotting these M scaled vectors on a coordinate system of scale a versus time or position t results in a wavelet scalogram of size $M \times N$.

In wavelet analyses, the choice of the mother wavelet is an important step, with the mother wavelet resembling the data as closely as possible (Smith et al., 1998; Lau and Weng, 1995; Weng and Lau, 1994). We follow the strategy of Gaucherel (2002) and Smith et al. (1998) and use the Mexican Hat wavelet as shown in Fig. 3 to analyze the hourly streamflow. We select the same waveform to analyze the hourly time series of mean areal rainfall derived from NEXRAD 4 km × 4 km gridded rainfall estimates.

An early comment regarding wavelet analysis was that it is apparently difficult to generate quantitative
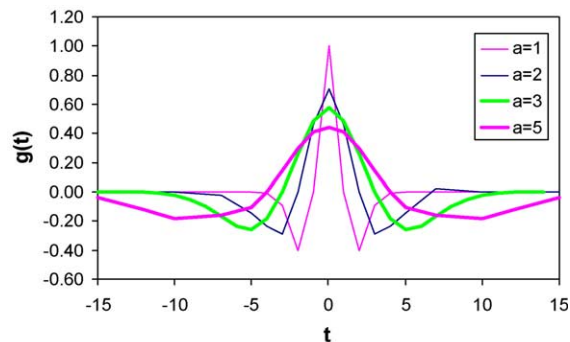
Fig. 3. Normalized approximations of the 'Mexican Hat' wave form showing the dilation that occurs as the scale a increases from 1 to 5.

results (Torrence and Compo, 1998; Meyers et al., 1993). Often, studies visually compared contoured plots of the wavelet coefficients to note the difference between signals (e.g. Weng and Lau, 1994). Labat et al. (2000b) used wavelet analysis to make qualitative statements about the filtering of high-frequency rainfall components by a karstic basin. In particular, the authors performed a wavelet decomposition of a single isolated rainfall-runoff event, leading to qualitative statements about the agreement between the large-scale (low-frequency) components of the rainfall and runoff signals. This latter analysis appears, at least on the surface, to provide the same smoothing effect as that seen in the work of Morin et al. (2002) for the computation of a basin RTS.

In our analysis, we go further to define a quantitative index that describes the variability in streamflow discharge in terms of filtering of the rainfall signal for an event. We base this index on the interpretation that the wavelet coefficients in the *MxN* transform matrix correspond to the correlation between the wavelet and the signal.

To derive the discharge variability index, the $M \times N$ transform of the signal $s(t)$ is scanned to locate the maximum wavelet coefficient at each time t, indicating the global 'spine' of the matrix. The points forming the spine correspond to the maximum correlation between the signal and wavelet. Meyers et al. (1993) analyzed points along the spine of several transformed signals to compute the dispersion of Yanai ocean waves. Here, we locate the minimum scale of the spine in the region of the hydrograph or hyetograph. We interpret this scale as the amount of dilation of the mother wavelet needed to achieve the best fit between the wavelet and the signal. Fig. 3 shows the dilation of the wavelet as the scale *a* increases. Moreover, we interpret this minimum wavelet scale to be a characteristic descriptor of the signal in this region.

Another way to interpret maximum wavelet coefficients along the spine is that these are the scales that have the highest energy at their corresponding time. In other words, the maximum coefficients represent the scales that contribute most significantly to the streamflow hydrograph at each of the corresponding hydrograph ordinates.

We define the variability in the observed discharge hydrograph by relating it to the rainfall by proposing

the event dampening ratio in Eq. (7):

$$R_d = \frac{\text{min\_scale}_{\text{discharge}}}{\text{min\_scale}_{\text{rainfall}}} \tag{7}$$

where $\text{min\_scale}_{\text{discharge}}$ and $\text{min\_scale}_{\text{rainfall}}$ are the minimum wavelet scales of the spine in the region of the event hydrograph and hyetograph, respectively. Large values of R_d indicate a relatively greater amount of dampening of the rainfall input signal.

Like the RTS statistic developed by Morin et al. (2002), the R_d statistic defined here has the advantage of using observed rather than modeled data. Moreover, it is independent of both the magnitude of the signal and also of the relative timing of the hyetograph and discharge hydrograph. Lastly, the R_d statistic avoids the need for baseflow separation, which can be a subjective process.

We apply this technique to the analysis of concurrent time series of hourly mean areal rainfall and observed streamflow for several basins. For this part of the analysis, we selected rainfall/runoff events meeting several criteria. First, as much as possible, isolated events were selected in which rainfall hyetograph and corresponding discharge hydrograph needed to have a single peak. Also, we selected events covering a range of magnitude and initial conditions in order to understand the range of dampening that occurs. Using these criteria, we were able to identify between 20 and 30 events for the Blue, Eldon, and Watts basins. Time series containing the specific events were created with length around 1000 h. In many cases, we were able to extract event time series of sufficient length. In other cases, we padded the discharge and rainfall time series with constant values flow and zeros, respectively, before and after the event. This step created sufficient room for waveforms of scale 128 and smaller to pass through without inducing edge effects which distort the wavelet coefficients. Subsequent wavelet analysis of these same events as they appeared in a multiyear time series led to the same minimum scales in the vast majority of cases. In the remaining cases, the analysis picked up the influence of nearby events. In such instances, we chose to retain the minimum scales from the event analysis.

As an example of these analyses, consider the storm event of September 28, 1995 that occurred over the Blue River Basin. The observed peak discharge for this
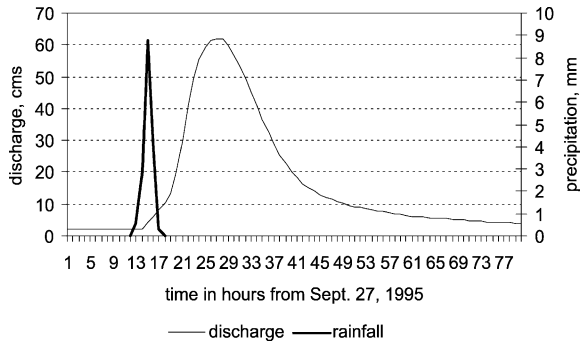
Fig. 4. Observed rainfall hyetograph and outlet hydrograph for example computation of dampening ratio.

event is 61 cms, while the rainfall occurred over a 5 h period and totaled 16.6 mm as shown in Fig. 4.

In this case, the Mexican Hat wavelet with scales a ranging from 1 to 32 was used to transform the discharge time series. Fig. 5 presents a 3-dimensional (3D) plot of the absolute value of the wavelet coefficients computed from the discharge time series. Time is plotted on the x axis and scale is plotted on the y axis. The wavelet coefficients rise out of the $x-y$ plane. It can be seen that a ridge of high coefficient values is present at approximately $t = 450$, indicating a region of good agreement between the discharge signal and the wavelet form.

The surface in Fig. 5 is then scanned to locate the maximum wavelet coefficient at each time step, thereby delineating the transform spine. For ease of visual interpretation and checking, the surface is also contoured as a two-dimensional (2D) plot. Fig. 6
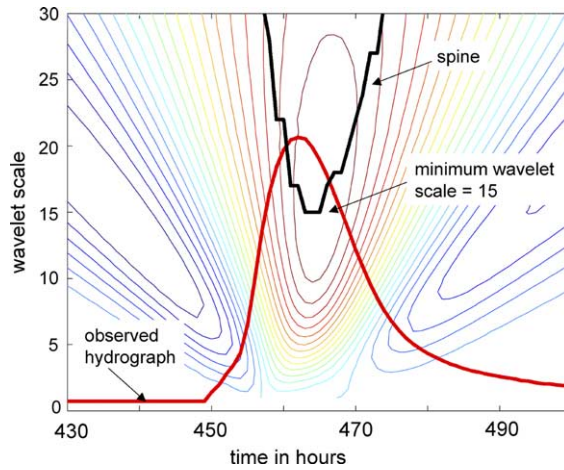
Fig. 6. Contours of wavelet coefficients for the Blue River event of September 28, 1995. The contours show a maximum around time 460 h. The spine of the matrix is plotted in black and shows a minimum scale of 15. The hydrograph (ordinates divided by 3) is plotted for clarity using the same y axis scale as the wavelet scale.

presents an enlargement of the contoured region around $t = 450$. In addition, the discharge hydrograph is plotted at 1/3 scale to help the reader orient the spine to the original hydrograph. The contours in Fig. 6 show locations of equal wavelet coefficients, and confirm the location of the spine, which has a minimum value of 15. We interpret this to mean that a Mexican Hat wavelet with a scale of 15 is the best descriptor of the discharge hydrograph in this vicinity. In other words, the value of the spine in Fig. 6 represents physically the scale corresponding
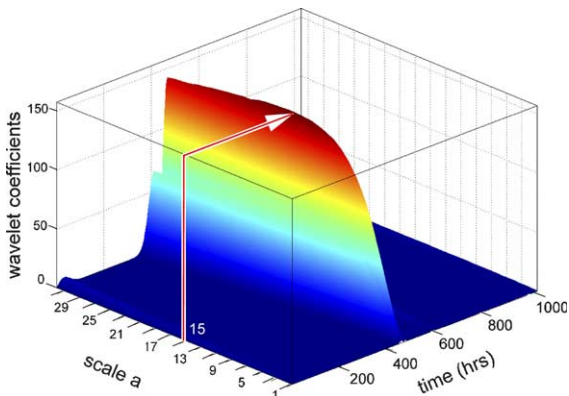
Fig. 5. Absolute value of wavelet coefficients for the observed discharge, Blue River, September 28, 1995. Wavelet coefficients rise out of the scale-time plane.
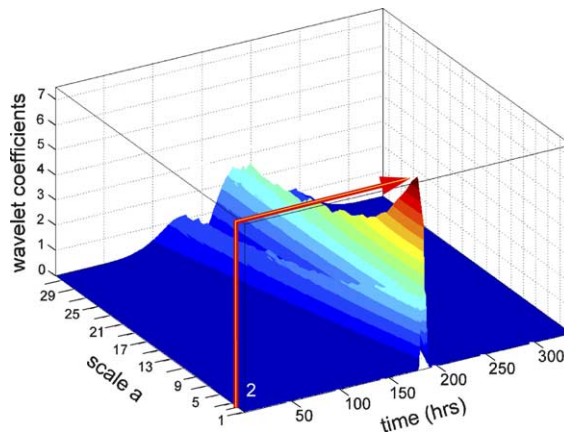
Fig. 7. Absolute value of the wavelet coefficients for the rainfall signal, Blue River, September 28, 1995 event.
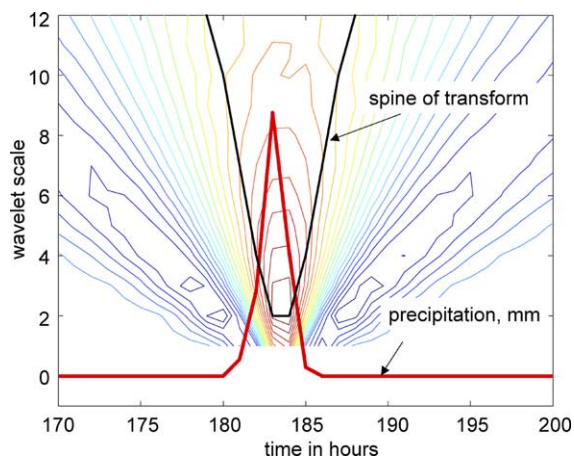
Fig. 8. Contours of wavelet coefficients for the rainfall hyetograph for the Blue River event of September 28, 1995. The spine of the matrix is plotted in black and shows a minimum scale of 2. The rainfall hyetograph is plotted for clarity using the same y axis scale as the wavelet scale.

to the highest frequency among the scales that have highest energy at each time step. Also, the scale from Fig. 6 represents the scale that contributes the most (in a sense) to the high-frequency of the corresponding hydrograph signal.

Similar analyses are performed on the hourly time series of mean areal rainfall for the September 28, 1995 event. The corresponding 3D and contour plots are shown in Figs. 7 and 8, respectively. The resultant value of the dampening ratio R_d is 15/2 or 7.5.

We provide an independent check of our method of wavelet analysis of isolated rainfall hyetographs and discharge hydrographs. Because of the single-peaked nature of these event signals, we seek to ensure that the analyzing wavelet filters out the requisite frequency range of the rainfall or discharge signal. To check our use of wavelets in this case, we compare the power spectral densities (PSDs) of the signal and the corresponding 'best fit' dilated wavelet. The PSDs of the best fit wavelet and the signal should peak in the same frequency range for the wavelet analysis to have physical meaning.

For this analysis, we select the rainfall event of October 9, 1994. PSD functions were computed for both the best fit (scale 3) Mexican Hat wavelet and mean areal rainfall hyetograph. In both cases, the time series length was 64 h and the maximum lag was 20 h.

Following the method presented in Kisiel (1969, see pp. 79–83) and later Torrence and Compo (1998), confidence limits for both the hyetograph and Mexican Hat power spectra were derived using a white noise null continuum. A white noise spectrum was used as a null continuum whose spectral density was constant and equal to the average of the values of all spectral estimates in the computed spectra of the Mexican Hat wavelet or hyetograph. 95% and 5% confidence limits were estimated from a χ^2 distribution with six degrees of freedom ($v = (2N - k/2)/k$, where v is the degrees of freedom, N is the time series length, and k is the number of time lags). Fig. 9 displays the PSD plots for the rainfall hyetograph of October 9, 1994 and the best fit wavelet (scale 3). It can be seen from Fig. 9 that there is good frequency correspondence between the statistically significant power for both signals.
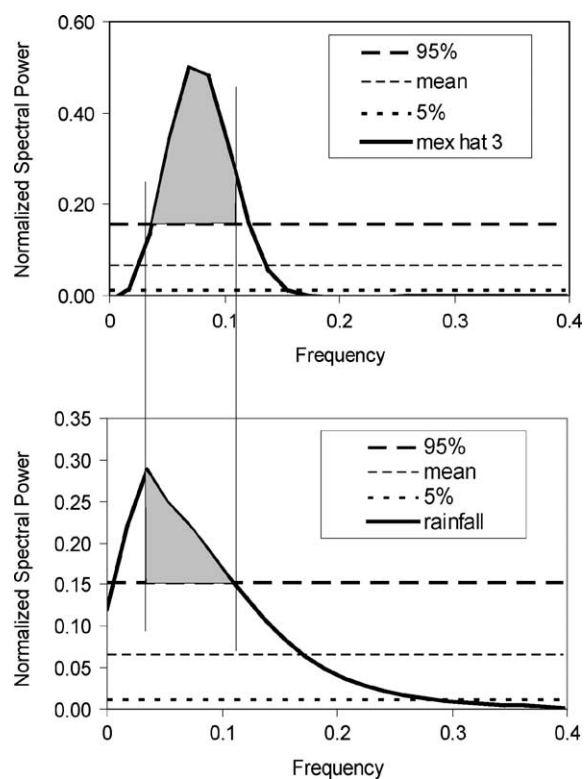
Fig. 9. Power Spectral Density plots of the rainfall for the October 9, 1994 event (bottom) and the corresponding 'best fit' Mexican Hat waveform of scale 3 (top). Shaded areas show that the majority of the statistically significant variance or power (>95%) for both curves lies within the same frequency band.
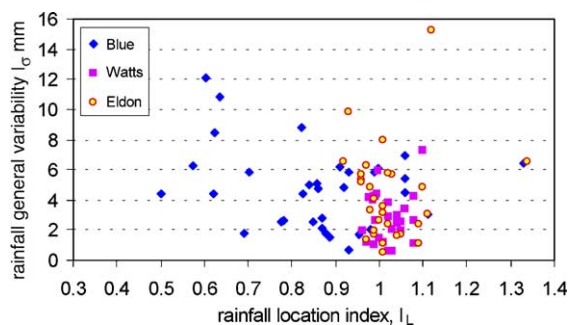
Fig. 10. Location index versus general variability index for three basins.

5. Results and discussion

5.1. Analysis of observed rainfall and streamflow

In this section, we compute the indices described in the previous sections in order to understand the nature of the rainfall variability and its effect on the basin outlet discharge variability. These indices are computed for 23, 25, and 31 rainfall/discharge events for Watts, Eldon, and Blue, respectively.

Fig. 10 presents the relationship between the locational variability and general variability of rainfall for the three basins using the events selected for wavelet analysis. For basin Watts, the data points fall within a very narrow range of I_L, say 0.95–1.1. Basin Watts also exhibits the smallest range of I_σ, with all of the data points falling below a value of 8 for I_σ. With the exception of one data point, basin Eldon exhibits a range of I_L values nearly as narrow as Watts. However, basin Eldon exhibits the largest range of general variability, with I_σ values extending to almost 16 mm. It should be noted that its range is characterized by a large gap between a solitary point at I_σ of about 16 and the next largest I_σ value of 10. In contrast to Watts and Eldon, basin Blue shows a very
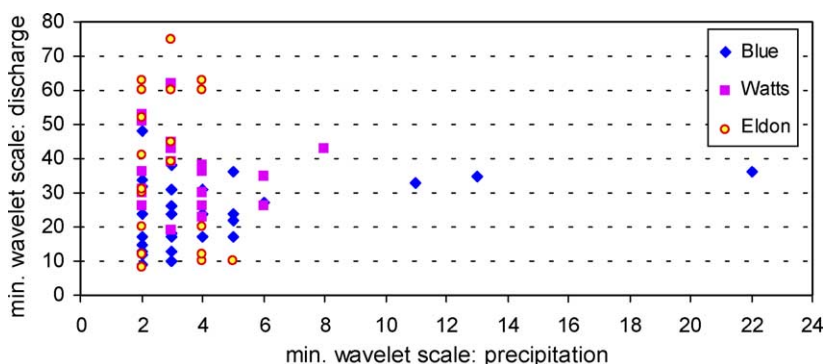
Fig. 11. Scatter plot of minimum wavelet scales for three basins.
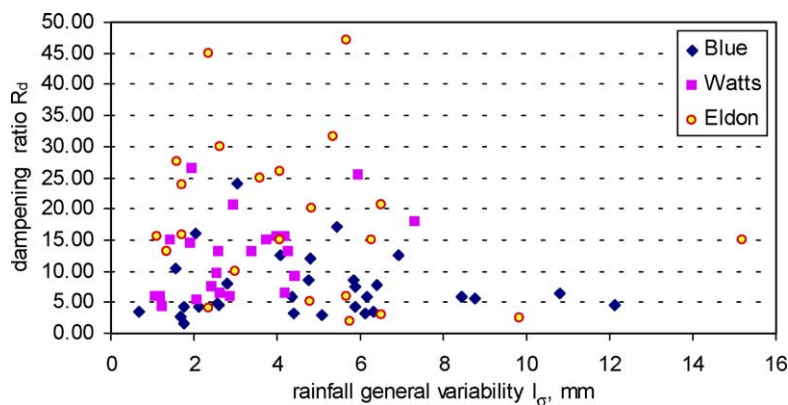
Fig. 12. Scatter plot of dampening ratio R_d versus general rainfall variability I_σ.

broad range of locational variability, with values of I_L extending from 0.5 to over 1.3. Based on the events plotted in Fig. 10, we can suggest that basin Watts contains the most spatially uniform rainfall patterns, followed by basin Eldon. The rainfall for basin Blue is the most spatially variable. It may be that data points outside these ranges exist for each basin, but did not meet the selection criteria for the wavelet analysis.

Fig. 11 can be used to describe the dampening performed by each basin. This figure displays the relationship between the wavelet scales characterizing the input rainfall signal and the output discharge hydrographs for the events in the three basins. While strong conclusions cannot be made from Fig. 11, it seems that inferences can nonetheless be suggested. At precipitation scales of 2, 3, 4, and 5 (corresponding to higher frequency events) it can be seen that all basins perform a range of dampening of the input rainfall shape. In particular, basin Eldon seems to exhibit a wide range of dampening response at each rainfall scale. Basin Blue has less of a dampening effect, indicating that the basin could be more sensitive to variations in precipitation. For each rainfall scale, the basin Watts exhibits a range of dampening nearly as narrow as that of Blue. It is interesting to note that Blue exhibits a much wider range of minimum wavelet scales of rainfall than the other two basins. Similar to Morin et al. (2002), we make no inferences regarding the reasons for the dampening (e.g. initial conditions, type of soils, rainfall/runoff mechanism, routing, etc.).

In Fig. 12, the wavelet scales are combined to form the dampening ratio R_d and plotted against the index of general rainfall variability I_σ. From this figure, it can be seen that the three basins exhibit a range of the general rainfall variability index I_σ. The range of values along the R_d axis is greatest for Eldon, with points falling between R_d values of 2–47. Basin Blue has less of a dampening effect at all values of I_σ with only three points having R_d of 15 or greater, again indicating that the basin could be more sensitive to variations in precipitation. At each I_σ scale, Blue seems to function in the same range or slightly lower than basin Watts. The mean of the cluster of points for Blue is slightly lower than Watts (7.4 and 12.3, respectively). Most importantly, there seems to be no identifiable or clear relationship between R_d and I_σ for the three basins.

Fig. 13 shows the relationship between the dampening ratio R_d and the index of locational rainfall variability I_L. It is immediately evident that distinguishable basin behavior is present. It can be seen from this plot that both Eldon and Watts basins have a limited range of the index of rainfall location I_L compared to basin Blue. With one exception, all of the points for basins Eldon and Watts fall within the bounds of $0.9 < I_L < 1.12$. Watts may have a slightly narrower range than Eldon. This range indicates that the rainfall is typically concentrated near the centroid of the basins (as defined by the overland and channel flow paths). Basin Blue exhibits great locational rainfall variability with values of I_L ranging from 0.5 to 1.33. Given the number of events concentrated between the outlet and centroid of the basin, it seems unusual that only one event having a locational index of greater than 1.1 occurred. It is conceivable that more such events exist, but did not meet the selection criteria for the wavelet analysis. For Blue, there is a slight trend for the value of R_d to increase as the location index increases. This trend seems logical in that longer flow distance may provide the channel system more opportunity to attenuate the runoff hydrograph. It should also be noted that at values of I_L between 0.9 and 1.1, Blue and Watts have a similar spread of R_d, with Blue having a somewhat smaller range. For I_L values outside this range, Blue has the smallest dampening effect on the input precipitation. This response suggests that Blue is sensitive to spatial patterns in rainfall so that variability in the input rainfall signal could be translated to variability in the runoff hydrograph.

Figs. 10–13 clearly show that different manifestations of rainfall variability are present in the three basins. Moreover, the three basins seem to exert varied degrees of dampening of the input rainfall signal. These analyses provide understanding as to how the basins generally respond to various degrees of spatial rainfall variability.

5.2. Analyses including DMIP simulation results

In this section, we rely on distributed and lumped model results to evaluate our hypothesis. As described by Reed et al. (2004, this issue), the results of DMIP showed a relative distributed modeling success that varied from basin to basin. Overall statistics showed
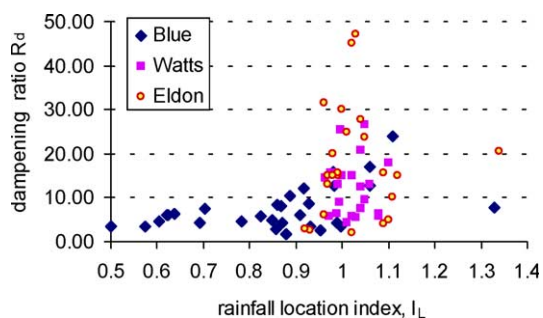
Fig. 13. Dampening ratio R_d versus rainfall location index I_L.

that in many cases, the lumped model had better performance than distributed models. However, some distributed models showed comparable or better performance for several events. In Fig. 14, we present a subset of the overall results and examine the gains from the NWS distributed model (see Koren et al., 2004) plotted versus the two indices of rainfall spatial variability for three basins. Distributed model gain is defined here as the difference in the Rmod statistic (NWS distributed minus NWS lumped) computed for the same events in the previous analyses. The Rmod
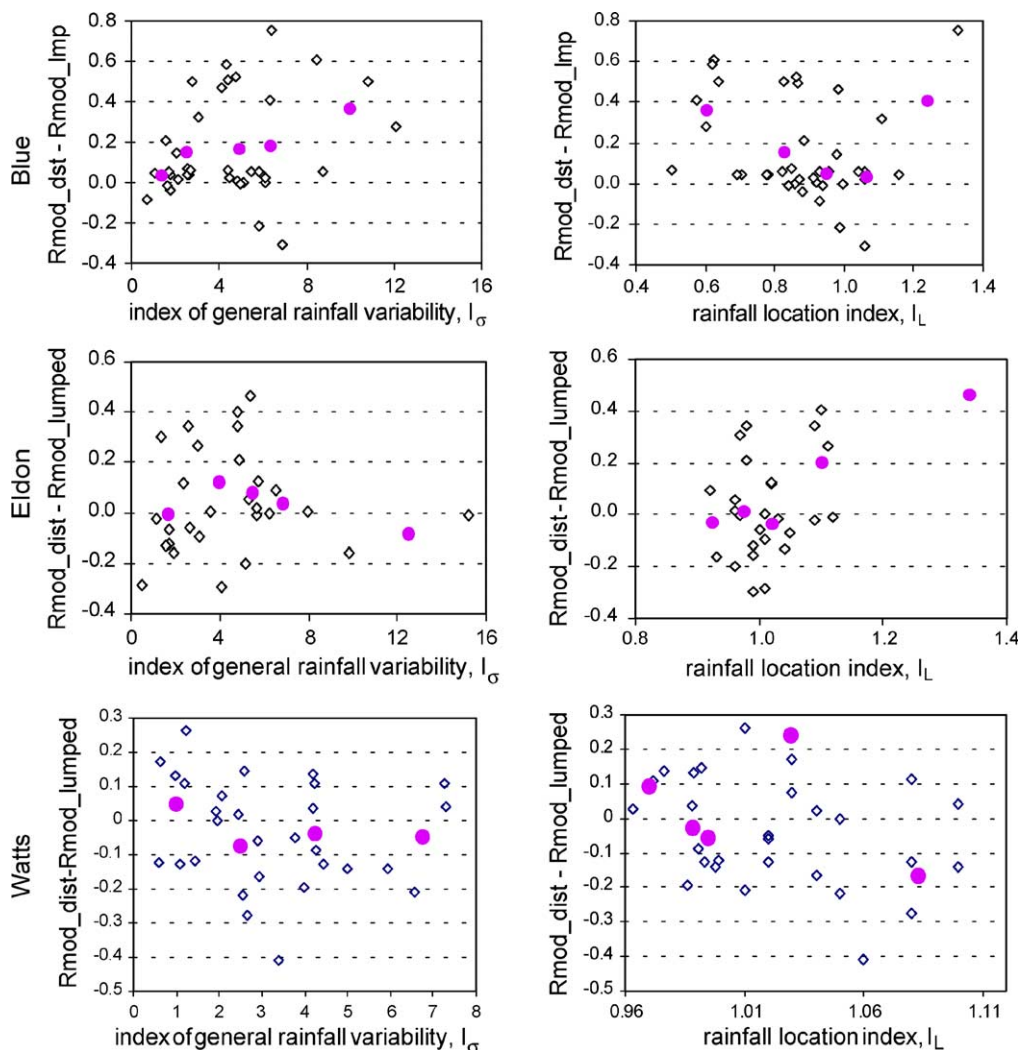
Fig. 14. Improvement of distributed model over lumped model versus locational variability and general rainfall variability for three basins: Blue (top), Eldon (middle), and Watts (bottom). The ordinate values are the difference in the event Rmod statistics (NWS distributed–NWS lumped). The large red dots represent average values within selected ranges of I_L and I_σ.

statistic is a modified correlation coefficient used in the evaluation of the DMIP results (Smith et al., 2004, this issue). Positive values on the ordinate indicate gain from distributed modeling, while negative values indicate loss of accuracy from distributed modeling. The large plotting symbols in Fig. 14 represent the average of the Rmod difference for successive intervals of I_σ and I_L. The following discussions will be based on these average values.

From the subplots in Fig. 14, it can be seen that the distributed model on average provides improvements over the entire range of I_σ values for basin Blue. As one would expect, the distributed model shows more gains as the I_L statistic varies from a value of 1.0, indicating high locational variability. These results suggest that the spatial variability of rainfall can be great enough to violate the conditions for lumped modeling to such a degree that distributed modeling is necessary to improve results. Or in the words of Obled et al. (1994), the rainfall can be sufficiently organized in space to overcome any filtering and dampening in the basin. Certainly, the low levels of dampening seen in Figs. 12 and 13 for Blue support this suggestion.

Fig. 14 also shows the Rmod difference between lumped and distributed simulations for Eldon. The results for Eldon show that the distributed model provided gains for about half the events. In contrast to Blue, the distributed model does not provide much improvement over the range of I_σ values. There is slight improvement (in an average sense) at I_σ values of 4 and 5, but a loss of accuracy at an I_σ value of around 12. Like basin Blue, there is some improvement as values of I_L increase from 1.0. However, it should be noted that the average value at I_L of 1.36 is based on a single point. Outside of this one event, the values of I_L cluster around 1.0, indicating that the rainfall is centered over the basin for the majority of events selected.

For Watts, distributed modeling provides only marginal improvement over lumped models at all ranges of I_L and I_σ values. Fig. 14 shows that any improvements were smaller than those for Eldon and Blue, with the difference in Rmod never greater than 0.3. As noted earlier, the range of I_L and I_σ values shown for Watts is the smallest of the three basins analyzed, indicating that the rainfall is more uniform. It is understandable that in such cases of uniform precipitation, it is difficult for a distributed model to

outperform a well-calibrated lumped model. Even though Watts behaves nearly the same as Blue in terms of the range of the dampening ratio R_d, there is apparently not enough variability in the input rainfall to generate variability in the basin runoff to the degree that a distributed model could be easily justified. Fig. 10 shows that Watts has the most spatially uniform precipitation of the three study basins. These results support the event statistics presented in Fig. 4 of Reed et al. (2004, this issue) which show that the calibrated lumped model performs rather well for Watts.

Figs. 15–17 further describe the events for which the NWS distributed model provides improvement. In these figures, we plot 3D data on 2D scatter plots. Two plotting symbols are used to denote a percent improvement gained by distributed modeling: a circle indicating positive improvements from the NWS distributed model and an inverted triangle to indicate negative values of the percent improvement (i.e. negative gain or degradation of simulation accuracy as a result of applying the distributed model). The relative size of the symbols for each basin indicates the magnitude of the gain or degradation compared to the NWS lumped model simulation. Comparing the relative sizes of the circles and triangles in Figs. 15–17 indicates that for the Blue River, distributed modeling provides great improvement for more events than for basins Eldon and Watts.

In Fig. 15, it can be seen again that the distributed model provides improvement at all ranges of the indices I_L and I_σ for basin Blue. Moreover, those events showing improvement are typically less dampened. With one exception, the events showing the largest improvement have a dampening ratio of less than 10. Distributed modeling does not provide improvements for the most dampened events. These events have I_L values of around 1.1 and I_σ values in the range of 3–5, respectively, indicating that the rainfall is fairly uniform. As stated earlier, it is usually difficult for a distributed model to improve upon a well-calibrated lumped model under these rainfall conditions. The relative size of the circles compared to the inverted triangles shows that a distributed model for Blue provides substantial improvement compared to a lumped model.
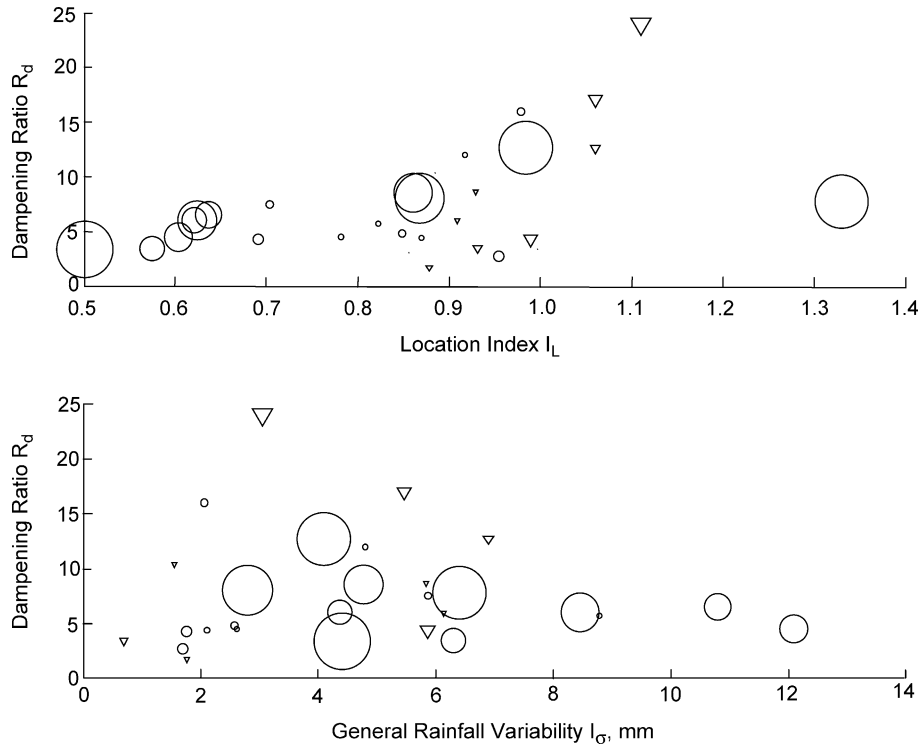
Fig. 15. Blue River (Blue): relative improvement of the NWS distributed model compared to the NWS lumped model plotted as a function of dampening ratio versus location index (top) and general variability (bottom). Circles represent improvement, inverted triangles represent degradation. The size of the plotting symbols shows the relative magnitude.

Figs. 16 and 17 show corresponding results for basins Eldon and Watts, respectively. As with basin Blue, it appears that the majority of events most benefiting from distributed modeling have a relatively low dampening ratio. Table 1 shows that the mean dampening ratios for positive distributed modeling gains are smaller than those for the negative distributed modeling gains.

6. Conclusions

Various analyses were conducted to evaluate our hypothesis that basins characterized by (1) significant spatial variability of rainfall and (2) less filtering of the rainfall signal will be amenable to distributed modeling for basin outlet simulations. To avoid model-specific conclusions, we tried as much as possible to base our analyses on observed data. However, we could not avoid using model results in evaluating our hypothesis.

Two indices of observed spatial rainfall variability and an index of observed basin filtering were computed for three basins within the DMIP study domain. These indices were combined with the results from the NWS distributed and lumped models used in DMIP.

Of the three basins and for the events studied, Blue exhibited the greatest rainfall variability, exhibiting prominent locational variability and a tendency for the rainfall patterns to be concentrated between the centroid and outlet of the basin. Considering both locational and general rainfall variability, precipitation for Eldon is the next most spatially variable, followed by Watts. We stress that more cases in which the rainfall is concentrated away from the basin centroid could exist for all three study basins, but did not meet the single peak event criteria for wavelet analysis.

An attempt was made to understand the filtering effects of each of three basins on the input rainfall signal. For this, we developed the event dampening
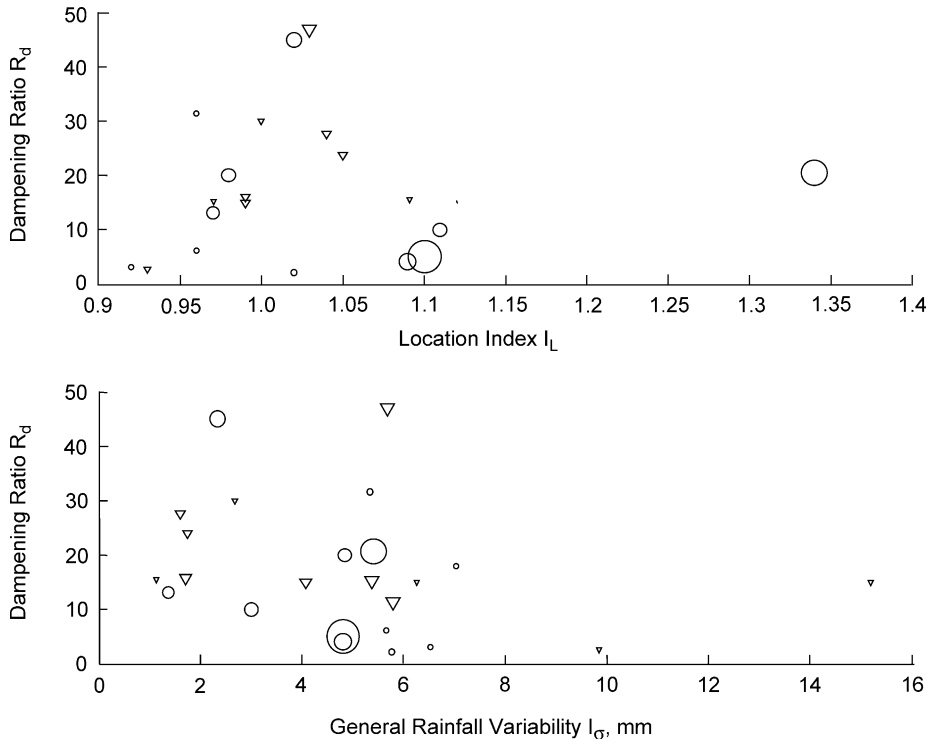
Fig. 16. Baron Fork at Eldon (Eldon): relative improvement of the NWS distributed model compared to the NWS lumped model plotted as a function of dampening ratio and location index (top) and general variability (bottom). Circles represent improvement, inverted triangles represent degradation. The size of the plotting symbols shows the relative magnitude.

ratio R_d, derived through wavelet analysis. The R_d statistic has the advantage of being computed from observed data and does not need baseflow separation, which can be a subjective procedure. Also, this dimensionless statistic is independent of magnitude and also the relative timing of the rainfall hyetograph and discharge hydrograph.

Once again, the basin Blue is distinguishable from Watts and Eldon, having the lowest event values of R_d, with a mean R_d of 7.4. Watts and Eldon follow with mean R_d values of 12.3 and 18.0, respectively. For Blue, we noticed a prominent trend for all events at the extremes of the location index I_L to be characterized by relatively low values of the dampening ratio R_d.

While we were unable to detect threshold values of the indices I_σ, I_L, and R_d which identify a basin amenable to distributed modeling, we nonetheless identified significant differences in the observed basin behavior. Within the scope of this study, we believe that our analyses support our hypothesis. We conclude

that basin Blue contains complexities that suggest the use of distributed models. Improvements were realized by distributed modeling over the entire range of storm center location for this basin.

It is interesting to note that basin Watts has the next lowest average dampening ratio after Blue. However, Watts had the least spatially variable rainfall. Based on the events in our study, we surmise that there is not enough spatial variability in the Watts rainfall to generate variable basin responses.

To the degree that the NWS distributed and lumped models are realistic and well-calibrated, we can conclude that when the observed rainfall patterns were more uniform (I_L values around 1.0 and relatively smaller I_σ values), the distributed model provided mixed results. In some cases, slight improvements over lumped model simulations were realized, in other cases the distributed model showed a small degradation in simulation accuracy. Not surprisingly, at I_L values far from 1.0, significant
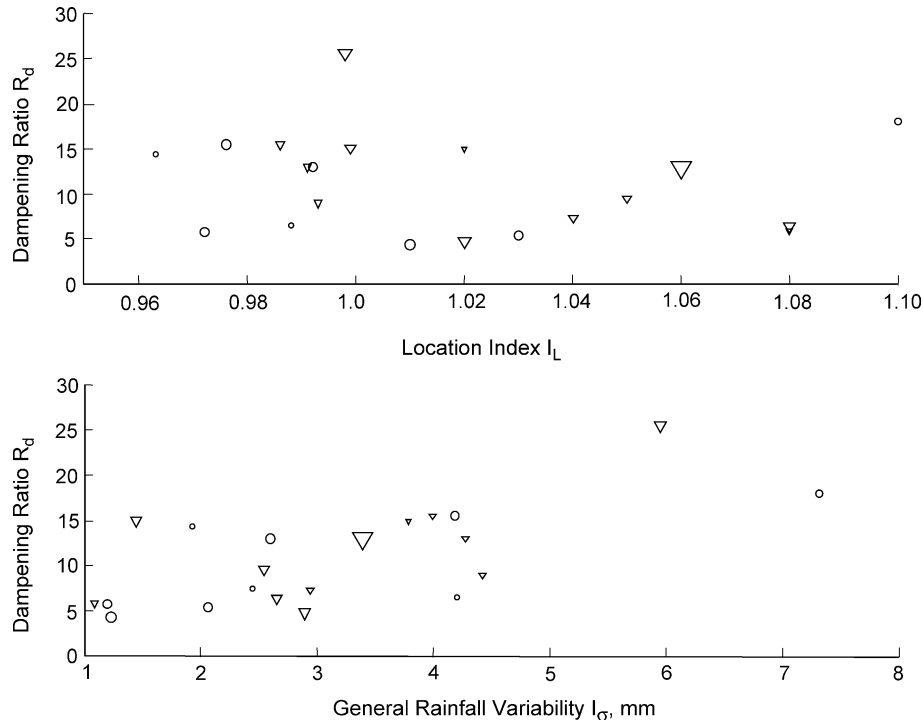
Fig. 17. Illinois River at Watts, OK (Watts): relative improvement of the NWS distributed model compared to the NWS lumped model plotted as a function of dampening ratio and index of locational variability (top) and general variability (bottom). Circles represent improvement, inverted triangles represent degradation. The size of the plotting symbols shows the relative magnitude.

improvements were realized in the Blue basin and to a lesser degree in Eldon. Strong relationships between distributed modeling improvement and values of I_σ cannot be seen for any basin.

7. Recommendations

Perhaps the first continuing efforts should focus on analyzing additional events beyond the scope of the DMIP calibration and validation periods. More data points would lead to a clearer understanding of the extent of rainfall variability and type of basin behavior. For all basins, it would be helpful to have more events with values of I_L greater than 1.0. Almost 2 years of data are now available beyond the end of the DMIP validation period. Given more data points, it would be also useful to stratify the analyses according to initial conditions, total storm precipitation, storm type, and peak discharge.

During the analysis of the rainfall data for basin Blue, we noted two trends. First, the rainfall patterns are such that rainfall rarely covers the entire basin. Rather than computing a time series of mean areal rainfall over the entire basin, it would be more representative to compute a conditional mean areal average (i.e. over only the rainy area). This would avoid some of the smoothing shown in Fig. 2 of Finnerty et al. (1997). Such a conditional analysis might decrease the minimum wavelet coefficient for

Table 1
Mean values of the dampening ratio R_d for the three study basins

Basin	Distributed modeling improvement	
	Positive	Negative
Blue	6.6	9.0
Eldon	15.4	20.7
Watts	10.0	12.8

Values are grouped as to whether distributed modeling realized improvements or losses compared to lumped modeling.

the precipitation, thereby increasing the dampening ratio. Second, we observed that many rainfall events in basin Blue are characterized by storms moving down the channel toward the outlet. Future work should include the study of observed storm movement in the computation of rainfall variability indices.

Other representations of the input rainfall signal may be necessary. Rather than using mean areal values for each time step to characterize the rainfall, perhaps a more refined representation of the rainfall can be derived from the gridded radar precipitation estimates.

Continuing the theme of Jakeman and Hornberger (1993), further analyses of the concurrent time series of rainfall and streamflow may yield more informative diagnostic indicators about the potential gain from distributed modeling. Wavelet decomposition of the concurrent time series of rainfall and streamflow may allow us to make inferences about the relative importance of low- and high-scale (high- and low-frequency) patterns in the data. Also, the signal analysis techniques discussed by Padilla and Pulido-Bosch (1995), Angelini (1997), Larocque et al. (1998), and Labat et al. (2000a,b) may provide additional overall descriptions of the input–output transformation in frequency–amplitude space.

It might also be informative to compute transfer functions for the events discussed here as well as additional events. Naden (1992) was able to compute such functions for seven events and make conclusions about the variability of the runoff hydrographs as well as the dominance of the hillslope or channel routing components. Such an analysis might partially confirm the wavelet approach applied to events in this study.

We also plan to examine other DMIP basins to gain a broader picture of how the dominance of locational and general rainfall may vary with basin scale. We suspect that locational variability may be dominant in larger catchments, with general rainfall variability becoming more important as basin size decreases.

For those instances in which distributed models are being considered for many areas, it would be beneficial to determine beforehand which basins might benefit most compared to a lumped approach for outlet simulations. Perhaps diagnostic criteria could be developed from observed data so as to identify and prioritize basins for distributed model implementation. Such a prioritization might realize the greatest gain for the resources expended. Such efforts would seem to be most important to agencies that are transitioning from simpler lumped methods to distributed models for operational river forecasting.

References

Angelini, P., 1997. Correlation and spectral analysis of two hydrogeological systems in Central Italy. Hydrological Sciences Journal 42(3), 425–438.

Arnaud, P., Bouvier, C., Cisneros, L., Dominquez, R., 2002. Influence of rainfall spatial variability on flood prediction. Journal of Hydrology 260, 216–230.

Bell, V.A., Moore, R.J., 1998. A grid-based distributed flood forecasting model for use with weather radar data. Part 2. Case studies. Hydrology and Earth System Sciences 2(3), 283–298.

Bell, V.A., Moore, R.J., 2000. The sensitivity of catchment runoff models to rainfall data at different spatial scales. Proceedings of the Conference on Hydrology and Earth System Sciences, Special Issue on HYREX: the Hydrological Radar Experiment 4(4), 653–667.

Berger, K.P., Entekhabi, D., 2001. Basin hydrologic response relations to distributed physiographic descriptors and climate. Journal of Hydrology 247, 169–182.

Beven, K.J., Hornberger, G.M., 1982. Assessing the effect of spatial patterns of rainfall in modeling stream flow hydrographs. Water Resources Bulletin 18(5), 823–829.

Cahill, A.T., 2002. Determination of changes in streamflow variance by means of a wavelet-based test. Water Resources Research 38(6), doi: 1029/2000WR000192.

Carpenter, T.M., Georgakakos, K.P., 2004. Impacts of parametric and radar rainfall uncertainty on the ensemble simulations of a distributed hydrologic model. Journal of Hydrology, 298(1–4), 202–221.

Carpenter, T.M., Georgakakos, K.P., Sperfslage, J.A., 2001. On the parametric and NEXRAD-radar sensitivities of a distributed

hydrologic model suitable for operational use. Journal of Hydrology 253, 169–193.

Finnerty, B.D., Smith, M.B., Seo, D.-J., Koren, V., Moglen, G.E., 1997. Space–time sensitivity of the Sacramento model to radar-gage rainfall inputs. Journal of Hydrology 203, 21–38.

Gaucherel, C., 2002. Use of wavelet tansform for temporal characterization of remote watersheds. Journal of Hydrology 269, 101–121.

Guo, J., Liang, X., Leung, R., 2004. Impact of different precipitation data sources on water budget simulated by the VIC-3L hydrologically-based land surface model. Journal of Hydrology, 298(1–4), 311–344.

Jakeman, A.J., Hornberger, G.M., 1993. How much complexity is warranted in a rainfall-runoff model? Water Resources Research 29(8), 2637–2649.

Kisiel, C.C., 1969. Time series analysis of hydrologic data. Advances in Hydroscience, vol. 5. Academic Press, New York, pp. 1–119.

Koren, V., Reed, S., Smith, M., Seo, D., Moreda, F., Kuzmin, V., 2003. Use of spatially variable data in river flood prediction. EGS/AGU Joint Conference, Nice, April 4–9, NH4-IMO4P-1414.

Koren, V., Reed, S., Smith, M., Zhang, Z., Seo, D.-J., 2004. Hydrology laboratory research modeling system (HL-RMS) of the US national weather service. Journal of Hydrology, 291, 297–318.

Krajewski, W.F., Lakshmi, V., Georgakakos, K.P., Jain, S.C., 1991. A Monte-Carlo study of rainfall sampling effect on a distributed catchment model. Water Resources Research 27(1), 119–128.

Kumar, P., Foufoula-Georgiou, E., 1990. Analyzing radar depicted rainfall fields using wavelet transforms. Proceedings of the Eighth Conference on Hydrometeorology, 22–26 October, Alta, Canada, Paper 7.5, pp. 175–178.

Kumar, P., Foufoula-Georgiou, E., 1993. A multi-component decomposition of spatial rainfall fields 1. Segregation of large- and small-scale features using wavelet transforms. Water Resources Research 29(8), 2515–2532.

Labat, D., Ababou, R., Mangin, A., 2000a. Rainfall-runoff relations for karstic springs. Part I. Convolution and spectral analysis. Journal of Hydrology 238, 123–148.

Labat, D., Ababou, R., Mangin, A., 2000b. Rainfall-runoff relations for karstic springs. Part II. Continuous wavelet and discrete orthogonal multiresolution analyses. Journal of Hydrology 238, 149–178.

Larocque, M., Mangin, A., Razack, M., Banton, O., 1998. Contribution of correlation and spectral analyses to the regional study of a large karst aquifer (Charente, France). Journal of Hydrology 205, 217–231.

Larson, J.E., Sivapalan, M., Coles, N.A., Linnet, P.E., 1994. Similarity analysis of runoff generation processes in real-world catchments. Water Resources Research 30(6), 1641–1652.

Lau, K.-M., Weng, H., 1995. Climate signal detection using wavelet transform: how to make a time series sing. Bulletin of the American Meteorology Society 76(12), 2391–2402.

Meyers, S.D., Kelly, B.G., O'Brien, J.J., 1993. An introduction to wavelet analysis in oceanography and meteorology: with applications to the dispersion of Yanai waves. Monthly Weather Review 121, 2858–2866.

Milly, P.C.D., Eagleson, P.S., 1988. Effect of storm scale on surface runoff volume. Water Resources Research 24(4), 620–624.

Morin, E., Enzel, Y., Shamir, U., Garti, R., 2001. The characteristic time scale for basin hydrological response using radar data. Journal of Hydrology 252, 85–99.

Morin, E., Georgakakos, K.P., Shamir, U., Garti, R., Enzel, Y., 2002. Objective, observations-based, automatic estimation for the catchment response time scale. Water Resources Research 38(10), 1212doi: 10.1029/2001WR000808.

Morin, E., Georgakakos, K.P., Shamir, U., Garti, R., Enzel, Y., 2003. Investigating the effect of catchment characteristics on the response time scale using a distributed model and weather radar data. Weather Radar Information and Distributed Hydrological Modeling. Proceedings of Symposium HS03 held during IUGG2003 at Sapporo, Japan. IAHS Publication No. 282, 177–185.

Naden, P., 1992. Spatial variability in flood estimation for large catchments: the exploitation of channel network structure. Hydrological Sciences Journal 37(1), 53–71.

Obled, C., Wedling, J., Beven, K., 1994. The sensitivity of hydrological models to spatial rainfall patterns: an evaluation using observed data. Journal of Hydrology 159, 305–333.

Ogden, F.L., Julien, P.Y., 1993. Runoff sensitivity to temporal and spatial rainfall variability at runoff and small basin scales. Water Resources Research 29(8), 2589–2597.

Padilla, A., Pulido-Bosch, A., 1995. Study of hydrographs of karstic aquifers by means of correlation and cross-spectral analysis. Journal of Hydrology 168, 73–89.

Pessoa, M.I., Bras, R.L., Williams, E.R., 1993. Use of weather radar for flood forecasting in the Sieve River Basin: a sensitivity analysis. Journal of Applied Meteorology 32(30), 462–475.

Reed, S.M., 2003. Deriving flow directions for coarse resolution (1–4 km) gridded hydrologic modeling. Water Resources Research 39(9), 1238 doi: 10.1029/2003WR001989.

Reed, S.M., Koren, V., Smith, M., Zhang, Z., Moreda, F., Seo, D.-J., and DMIP Participants, 2004. Overall distributed model inter-comparison project results. Journal of Hydrology, 298(1–4), 27–60.

Saco, P., Kumar, P., 2000. Coherent modes in multiscale variability of streamflow over the United States. Water Resources Research 36(4), 1049–1067.

Seyfried, M.S., Wilcox, B.P., 1995. Scale and the nature of spatial variability: field examples having implications for hydrologic modeling. Water Resources Research 31(1), 173–184.

Shah, S.M.S., O'Connel, P.E., Hosking, J.R.M., 1996. Modelling the effects of spatial variability in rainfall on catchment response. 1. Formulation and calibration of a stochastic rainfall field model. Journal of Hydrology 175, 67–88.

Shanholtz, V.O., Ross, B.B., Carr, J.C., 1981. Effect of spatial variability on the simulation of overland and channel flow. Transactions on ASAE 24(1), 124–138.

Smith, L.C., Turcotte, D.L., Isacks, B.L., 1998. Stream flow characterization and feature detection using a discrete wavelet transform. Hydrological Processes 12, 233–249.

Smith, M., Koren, V., Finnerty, B., Johnson, D., 1999. Distributed modeling: phase 1 results. NOAA Technical Report NWS 44, February, 250 pp. (copies available upon request).

Smith, M.B., Seo, D.-J., Koren, V.I., Reed, S., Zhang, Z., Duan, Q.-Y., Cong, S., Moreda, F., 2004. The distributed model intercomparison project (DMIP): motivation and experiment design. Journal of Hydrology, 298(1–4), 4–26.

Torrence, C., Compo, G.P., 1998. A practical guide to wavelet analysis. Bulletin of the American Meteorological Society 79(1), 61–78.

Wang, D., M, B., Smith, Z., Zhang, S., Reed, V., Koren, V., 2000. Statistical comparison of mean areal precipitation estimates from WSR-88D, operational and historical gage networks, paper 2.17. 15th Conference on Hydrology, AMS, January 9–14, Long Beach, CA, USA, 107–110.

Wei, T.C., Larson, C.L., 1971. Effects of areal and time distribution of rainfall on small watershed runoff hydrographs. Bulletin 30, Water Resources Research Center, University of Minnesota Graduate School, 118 pp.

Weng, H., Lau, K.-M., 1994. Wavelets, period doubling, and time–frequency localization with application to organization of convection over the tropical western Pacific. Journal of the Atmospheric Sciences 51(17), 2523–2541.

Wilson, C.B., Valdes, J.B., Rodriguez-Iturbe, I., 1979. On the influence of the spatial distribution of rainfall on storm runoff. Water Resources Research 15(2), 321–328.

Winchell, M., Gupta, V.H., Sorooshian, S., 1998. On the simulation of infiltration and saturation excess runoff using radar-based rainfall estimates: effects of algorithm uncertainty and pixel aggregation. Water Resources Research 34(10), 2655–2670.

Woods, R., Sivapalan, M., 1999. A synthesis of space–time variability in storm response: rainfall, runoff generation, and routing. Water Resources Research 35(8), 2469–2485.

Young, C.B., Bradley, A.A., Krajewski, W.F., Kruger, A., Morrissey, M.L., 2000. Evaluating NEXRAD multisensor precipitation estimates for operational hydrologic forecasting. Journal of Hydrometeorology 1, 241–254.